Electronic Supplementary Material (ESI) for Journal of Materials Chemistry C.
This journal is © The Royal Society of Chemistry 2020

Supporting Information

Rationally Designed Piezoelectric Charge Polarity at Interfaces for Largely Improving Photodiode Performance by Piezo-Phototronic Effect

Fangpei Li, Wenbo Peng,* Zijian Pan, and Yongning He*

Content:

A. Fabrication procedures and fundamental characterizations of p-Si/i-ZnO thin film/n-ZnO nanowires array photodiodes

The fabrication procedures of the p-Si/i-ZnO thin film/n-ZnO nanowires array photodiode are as-below:

(1) Prepare a polished p-type silicon wafer (phosphorus doped, 5-10 Ω·cm, <100>). Ultrasonically clean it for 5 min in acetone, ethanol, deionized water, consecutively, and blow-dry it by high-purified N_2.

(2) Deposit a layer of ZnO thin film by the radio frequency magnetron sputtering. Use a 3-inch-diameter ZnO ceramic target. The sputtering power is set to 110 W at room temperature and the argon to oxygen ratio is 10:1 under 1.0 Pa with a time duration of 5 min.

(3) Ultrasonically clean the sample for 3 min in acetone, ethanol, deionized water, consecutively, and dry it by the high-purified N_2. The nutrient solution for hydrothermally growing ZnO NWs consists of 25 mM zinc nitrate and 12.5 mM hexamethylenetetramine per 100 mL deionized water. In order to get separated and long ZnO NWs, 5.4 mL ammonium hydroxide (Alfa Aesar) per 100 mL is added into the mixed solution. The container is then pre-heated at 95 °C for 1 hr in a mechanical convection oven. Then the sample is carefully immersed in the solution with the ZnO thin film layer facing down. At the same constant temperature another 1 hr heating is required to grow ZnO NWs of proper lengths. After cooling down the whole system, the sample is collected and repeatedly washed by the deionized water. Then it is dried by the high-purified N_2.

(4) Finally, ITO and Al are deposited as the top and the bottom electrodes by radio frequency magnetron sputtering at room temperature, respectively. Copper wires are connected to

the as-fabricated electrodes by silver pastes. The effective area of the HPD is 5 mm × 5 mm.

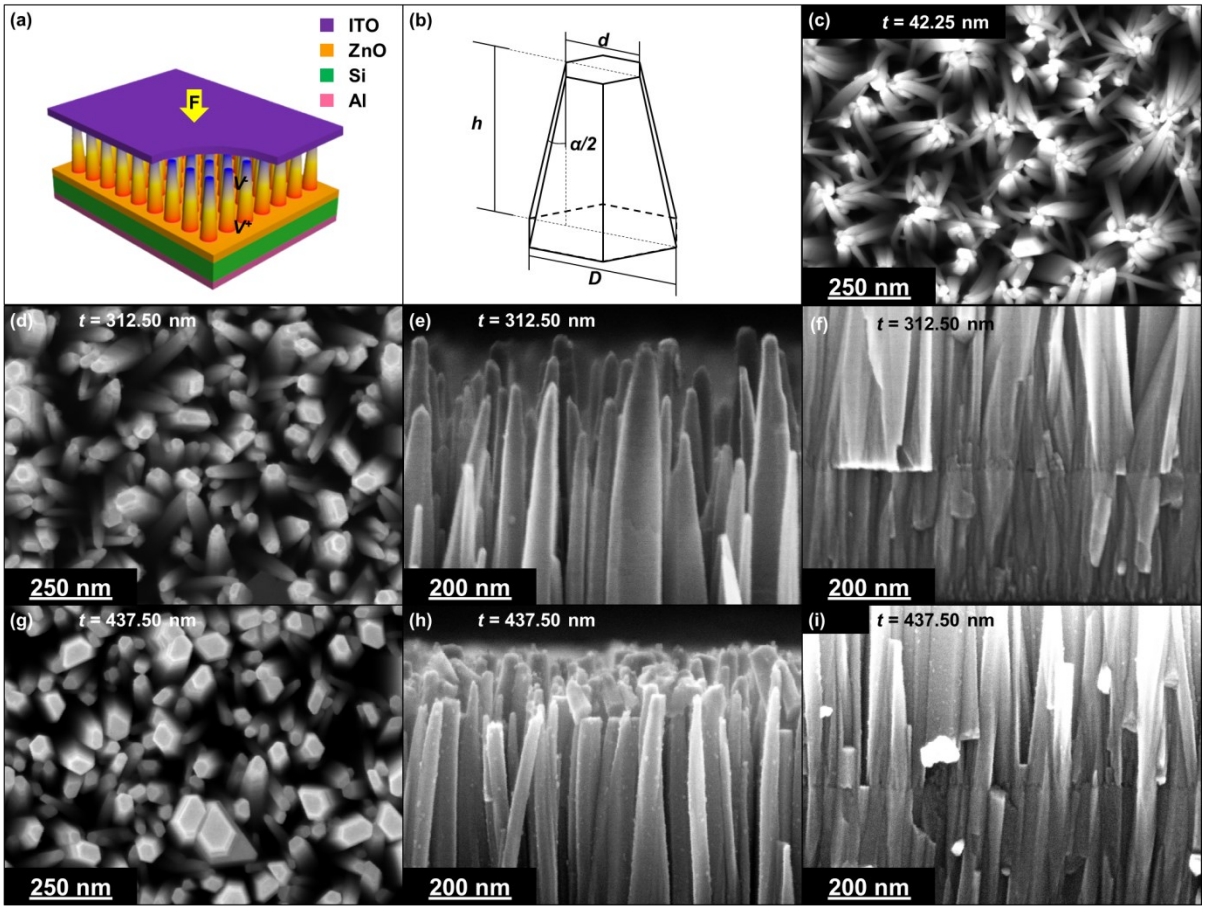

Fig. S1 **a** Schematic device structure of p-Si/i-ZnO thin film/n-ZnO nanowires array photodiode. **b** Illustrative sketch of ZnO single nanowire where necessary dimensional parameters are marked. **c** Top-view SEM image of DUT1. **d~f** Top-view and cross-sectional zoom-in SEM images of DUT2. **g~i** Top-view and cross-sectional zoom-in SEM images of DUT3.

B. Experiment apparatus, measurement system, and calculation of strain distribution in ZnO thin film and ZnO nanowires array

In order to generate, measure and record the electric signals, a precision source/measure

unit (B2902A, Keysight) is used here. The source sweeping voltage is set from -3 to 3 V with the Al electrode defined as the positive whereas the ITO electrode as the opposite. A continuously variable optical filter is used to tune the illuminant power intensity on the effective area of the device. The calculations of photoresponsivity and its relative changes are based on measured *J-V* results at a bias of -3 V.

The commercial finite element analysis (FEA) software COMSOL Multiphysics is utilized to conduct the theoretical simulation and calculation of the externally applied compressive strains within the ZnO thin film and ZnO nanowires array. According to the schematic experiment apparatus shown in Figure S2a and the device structure of the p-Si/i-ZnO thin film/n-ZnO nanowires array photodiode shown in Figure S1a, a three-dimensional (3D) model with exact the size of the practical device is constructed. The cross-sectional view of the 3D model is shown in Figure S2b. All the materials' parameters used in the simulation are listed below in Table S1. The nether surface of the bottom PMMA is fixed, which means it has no displacements in any directions at all. Then a downward displacement along the *c*-axis direction of the ZnO (*i.e.*, the *z*-axis direction in the coordinate) as a boundary condition is applied to the upper surface of the top glass to describe the externally applied compressive displacements in the experiments. An electric ground boundary condition is applied to the Al electrode which serves as the reference for the calculation of the piezo-potential distribution. Finally the piezoelectric constitutive equations are solved using Solid Mechanics, Electrostatics and Piezoelectric Effect modules in COMSOL. After the computation, the average strains and the piezo-potential distribution within ZnO thin film and ZnO NWs array under different compressive displacements can be derived and obtained by

post-processing.

Despite differences in morphology, other material properties such as Young's Modulus, densities, *etc.*, are set to the same in ZnO thin film and ZnO NWs array. However, when the device is under a prescribed compressive displacement, the strains generated within i-ZnO thin film and n-ZnO NWs array are different due to the larger piezoelectric coefficient of ZnO NWs[1]. Still, we use the average strain values by simulating i-ZnO thin film and n-ZnO NWs array as a whole in manuscript as well as in supporting information files for clear expression.

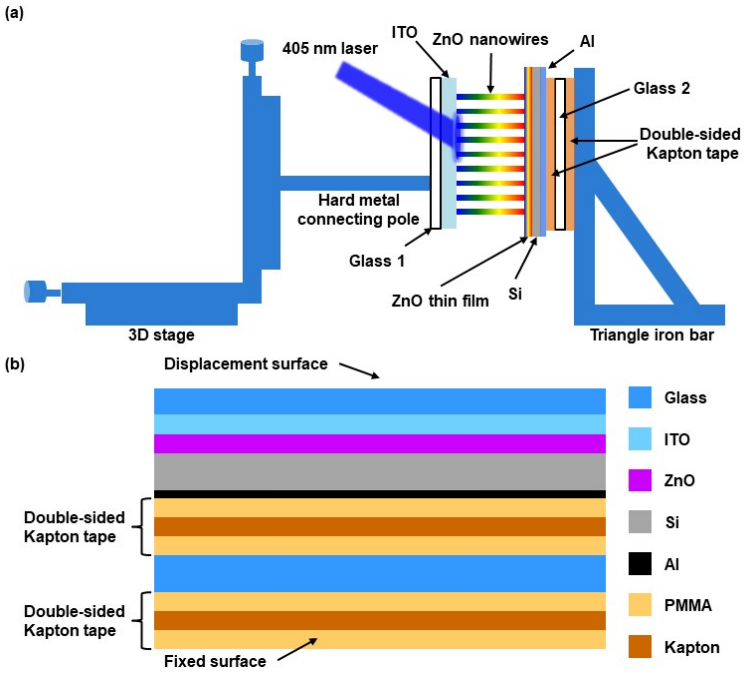

Fig. S2 a Schematic illustration of the experiment apparatus. **b** Cross-sectional view of the 3D simulation model.

Table S1 Materials' parameters used in the simulation.

Material	ε_r	Density (g/cm^3)	Young's modulus (GPa)	Poisson's ratio

Glass	2.09	2.20	73.1	0.17
PMMA	3.0	1.19	3.0	0.40
Kapton	3.4	1.30	3.1	0.34
ITO		6.80	116	0.35
Si	11.9	2.33	170	0.28
Al		2.70	70	0.35

C. Complementary photoresponse performances of p-Si/i- ZnO thin film/n-ZnO nanowires array photodiode

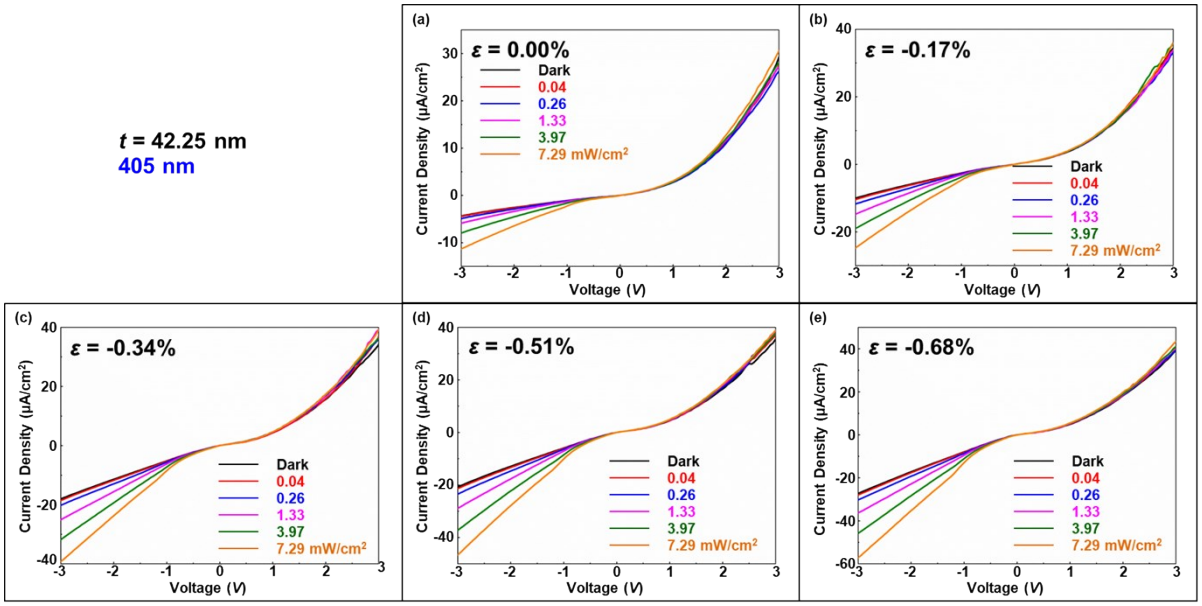

Fig. S3. Typical *J-V* curves of DUT1 to 405 nm laser illumination under different externally applied compressive strain: **a** ε = 0.00%, **b** ε = -0.17% **c** ε = -0.34%, **d** ε = -0.51%, and **e** ε = -0.68%. (Lines and symbols of different colors indicate different illuminant power intensities.)

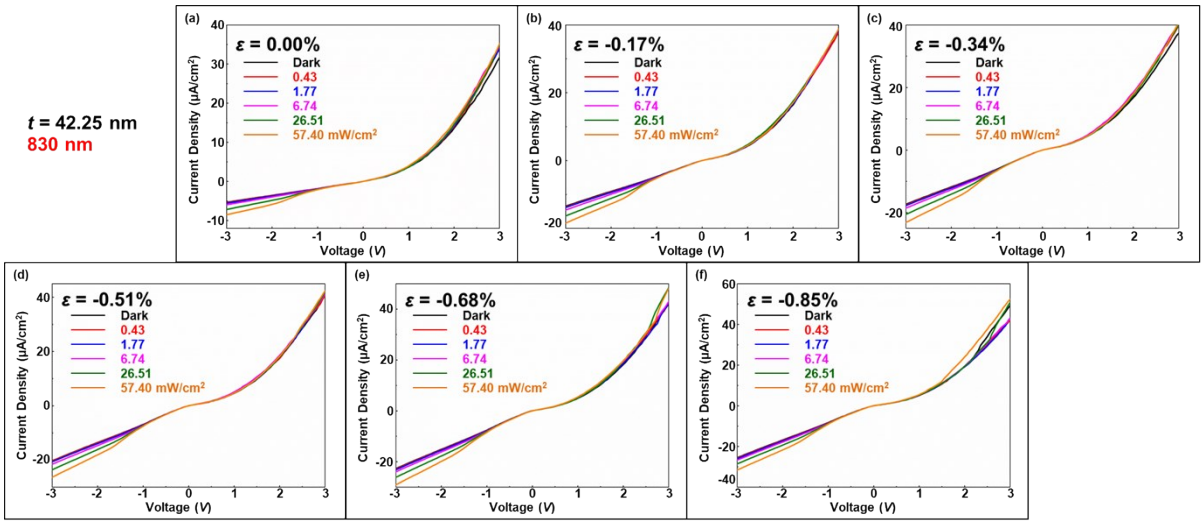

Fig. S4. Typical *J-V* curves of DUT1 to 830 nm laser illumination under different externally applied compressive strain: **a** ε = 0.00%, **b** ε = -0.17% **c** ε = -0.34%, **d** ε = -0.51%, **e** ε = -0.68%, and **f** ε = -0.85%. (Lines and symbols of different colors indicate different illuminant power intensities.)

D. Influence of thin film thickness on photoresponse performances modulated by piezo-phototronic effect

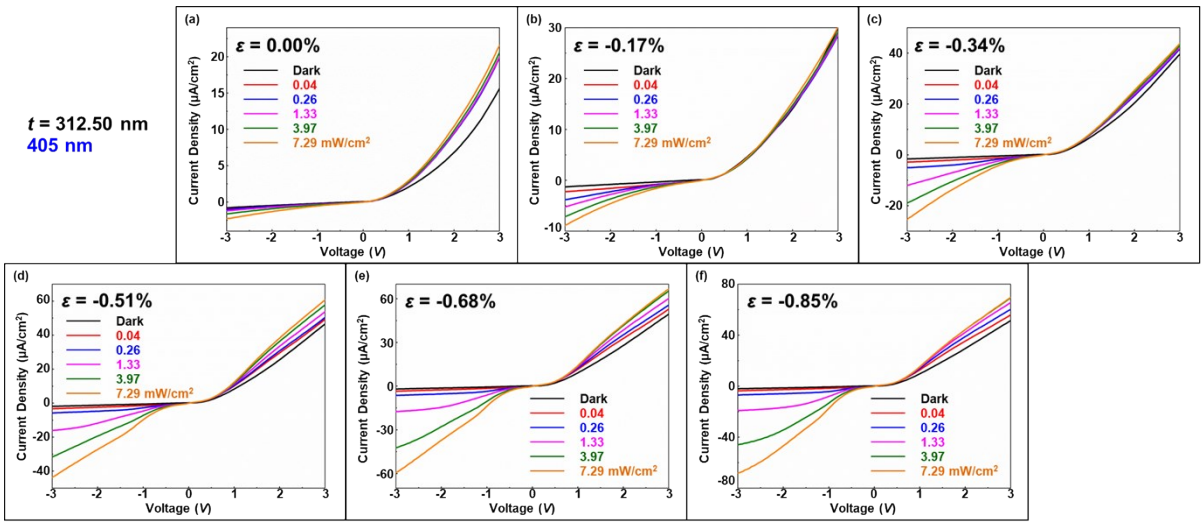

Fig. S5. Typical *J-V* curves of DUT2 to 405 nm laser illumination under different externally applied compressive strain: **a** ε = 0.00%, **b** ε = -0.17% **c** ε = -0.34%, **d** ε = -0.51%, **e** ε = -

0.68%, and **f** ε = -0.85%. (Lines and symbols of different colors indicate different illuminant power intensities.)

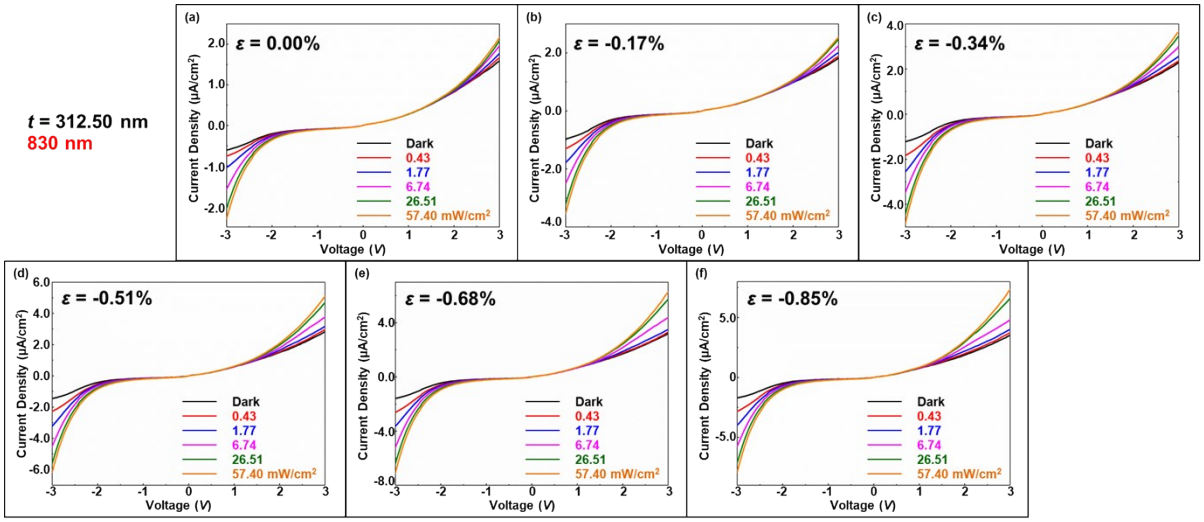

Fig. S6. Typical *J-V* curves of DUT2 to 830 nm laser illumination under different externally applied compressive strain: **a** ε = 0.00%, **b** ε = -0.17% **c** ε = -0.34%, **d** ε = -0.51%, **e** ε = -0.68%, and **f** ε = -0.85%. (Lines and symbols of different colors indicate different illuminant power intensities.)

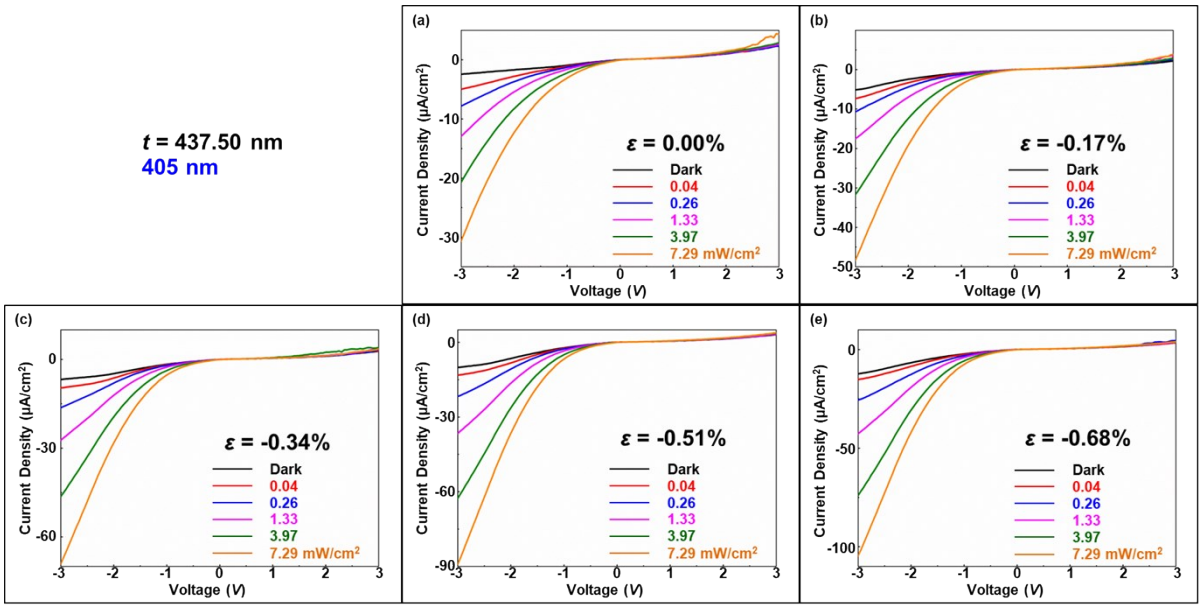

Fig. S7. Typical *J-V* curves of DUT3 to 405 nm laser illumination under different externally applied compressive strain: **a** ε = 0.00%, **b** ε = -0.17% **c** ε = -0.34%, **d** ε = -0.51%, and **e** ε =

-0.68%. (Lines and symbols of different colors indicate different illuminant power intensities.)

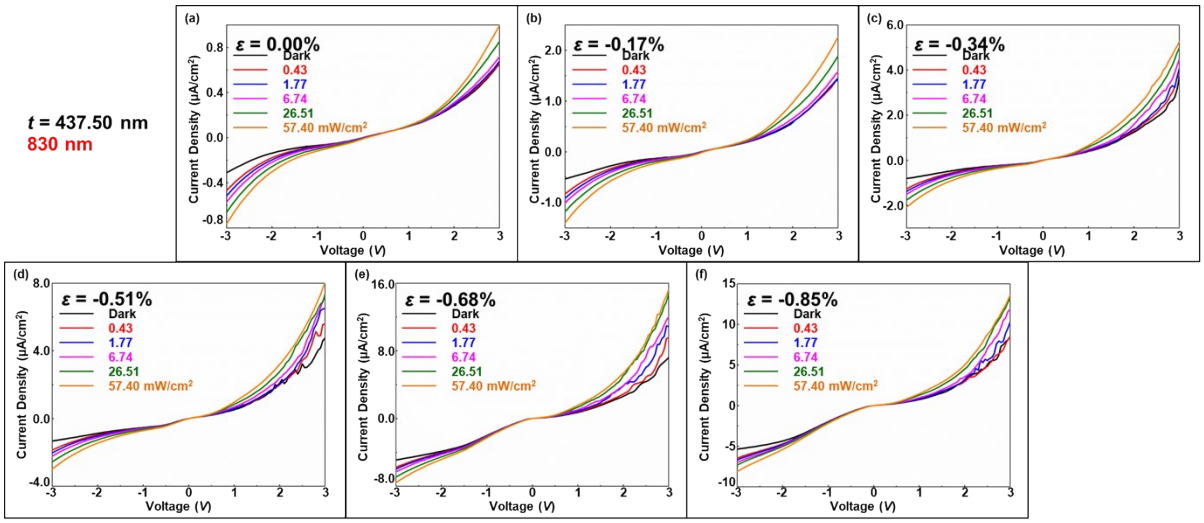

Fig. S8. Typical *J-V* curves of DUT3 to 830 nm laser illumination under different externally applied compressive strain: **a** ε = 0.00%, **b** ε = -0.17% **c** ε = -0.34%, **d** ε = -0.51%, **e** ε = -0.68%, and **f** ε = -0.85%. (Lines and symbols of different colors indicate different illuminant power intensities.)

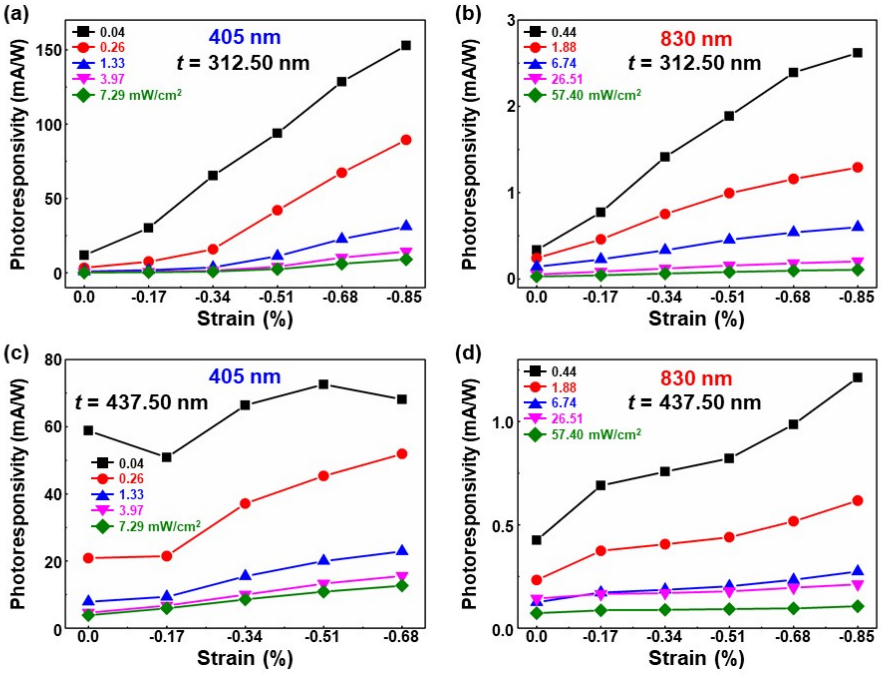

Fig. S9 Photoresponsivity of DUT2 as a function of externally applied compressive strain

under **a** 405 nm and **b** 830 nm laser illuminations, respectively. Photoresponsivity of DUT3 as a function of strain under **c** 405 nm and **d** 830 nm laser illuminations, respectively.

E. Transient photoresponse characteristics of p-Si/i- ZnO thin film/n-ZnO nanowires array photodiodes under strain free and strained conditions

The transient photoresponse characteristics of a photodiode are as desirable as its stationary photoresponse characteristics. Therefore here the typical transient photoresponse characteristics of DUT1, DUT2, and DUT3 are measured and recorded by the same precision source/measure unit (B2902A, Keysight) under a -2 V bias. A chopper is utilized here to "turn on" and "turn off" the laser illumination on the device at a fixed frequency of 10 Hz for both 405 and 830 nm laser illuminations. In Figure S10, the three sub-figures in the top row with blue background show the transient photoresponse characteristics of DUT1 under a 405 nm laser illumination with an illuminant power intensity of 7.29 mW/cm^2. Figure S10a and S10b demonstrate a typical cycle of transient photoresponse charcteristics at two representative externally applied compressive strains (*i.e.*, ε = 0.00% and ε = -0.85%), respectively. The rising edge as the laser illumination is "on" and the falling edge as the laser illumination is "off" are sharp and clear in both figures, distinctively showing the current density difference between the "on" and "off" states. Additionally, the rise and fall times of DUT1 under 405 nm laser illumination at different externally applied compressive strains are extracted, calculated and plotted in Figure S10c. Here, the rise time is defined as the time for the current density to increase from 10% to 90% of the maximum, and the fall time is defined as the time for the current density to decrease from 90% to 10% of the maximum. The three

sub-figures in the bottom row with pink background show the transient photoresponse characteristics under a 830 nm laser illumination with an illuminant power intensity of 57.40 mW/cm^2. Similarly, the rising and falling edges when the laser illumination is turned on and off under different externally applied compressive strains are sharp and clear (Figure S10d and S10e). The rise and fall times to 830 nm laser illumination as a function of externally applied compressive strain are also plotted in Figure S10f.

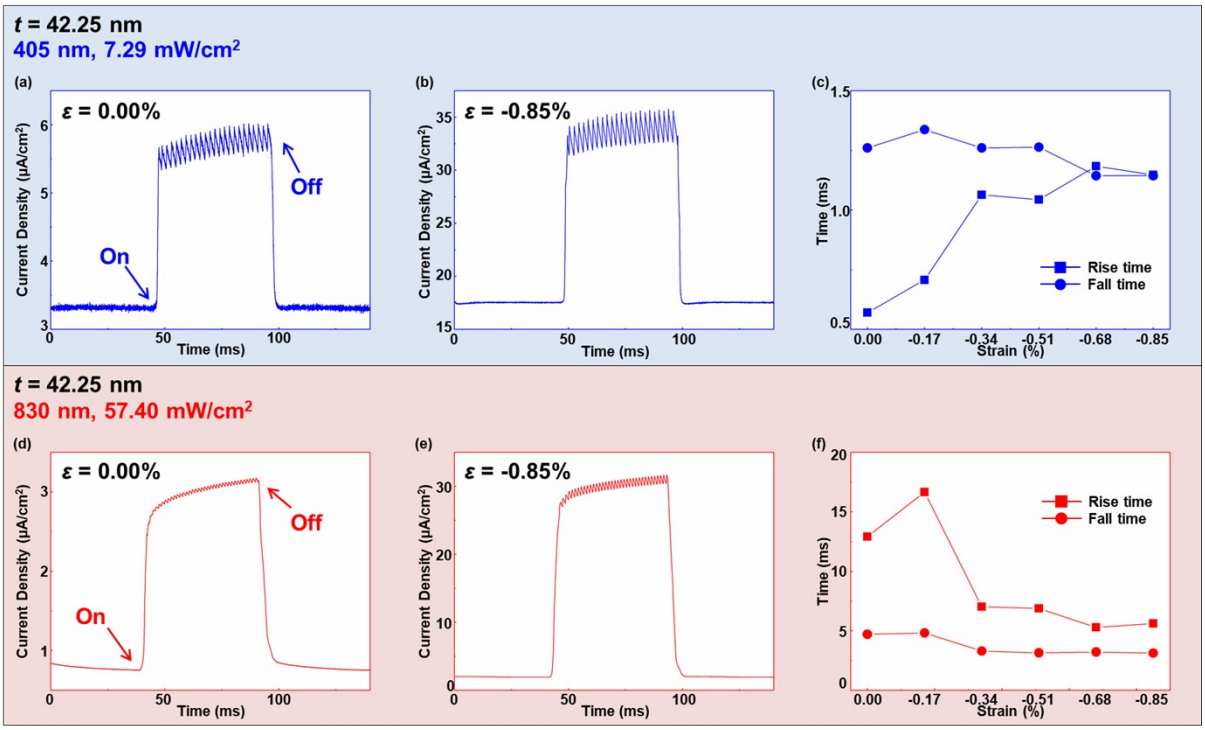

Figure S10. Transient photoresponse characteristics of DUT1. Under 405 nm laser illumination: **a** ε = 0.00%, **b** ε = -0.85%, and **c** rise and fall time as a function of externally applied compressive strain. Under 830 nm laser illumination: **d** ε = 0.00%, **e** ε = -0.85%, and **f** rise and fall time as a function of externally applied compressive strain. (Symbols of different shapes representing rise and fall times, respectively.)

Figure S11 and S12 give the transient photoresponse characteristics of DUT2 and DUT3

under both 405 and 830 nm laser illuminations. Basic phenomena can be concluded: under laser illuminations of both 405 and 830 nm, the transient photoresponses of all the devices are quite fast and distinguishable in spite of the changes in externally applied compressive strain. However, the strain-induced modulation in rise and fall times is not that clear. Still, the strained-induced modulations in stationary photoresponse characteristics are quite clear and formidable according to our experiments results and analyses.

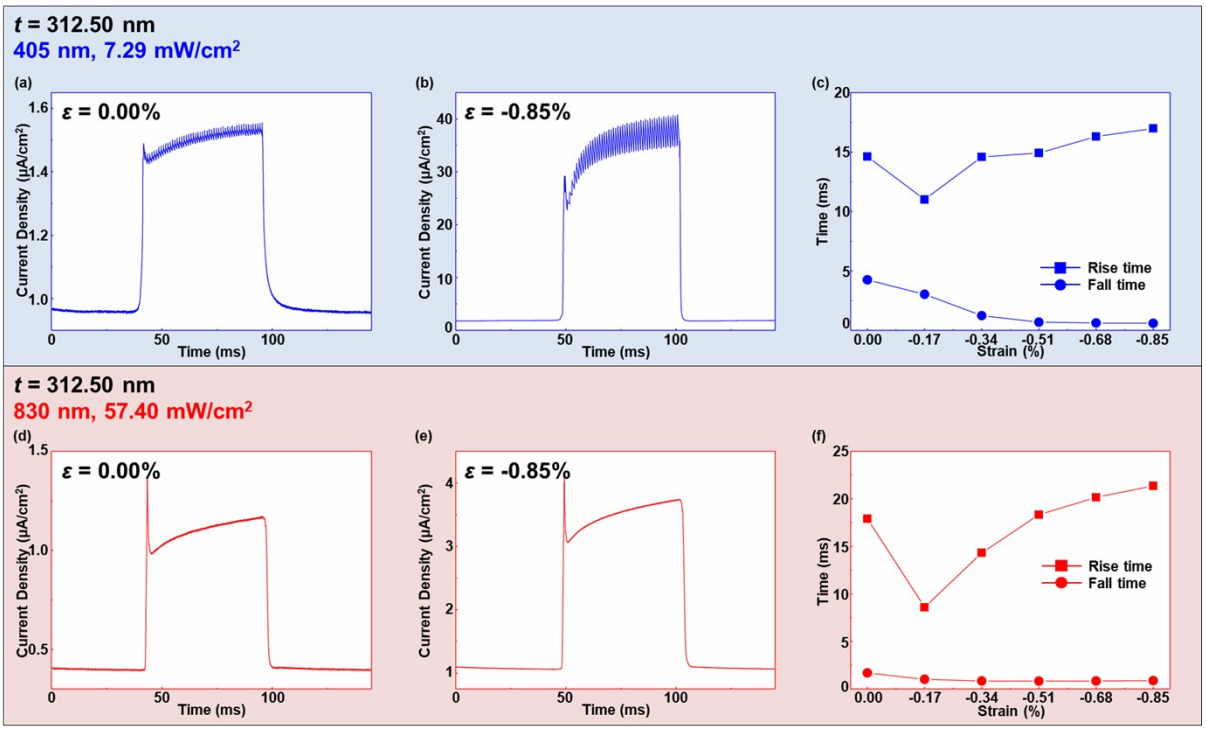

Figure S11. Transient photoresponse characteristics of DUT2. Under 405 nm laser illumination: **a** ε = 0.00%, **b** ε = -0.85%, and **c** rise and fall time as a function of externally applied compressive strain. Under 830 nm laser illumination: **d** ε = 0.00%, **e** ε = -0.85%, and **f** rise and fall time as a function of externally applied compressive strain. (Symbols of different shapes representing rise and fall times, respectively.)

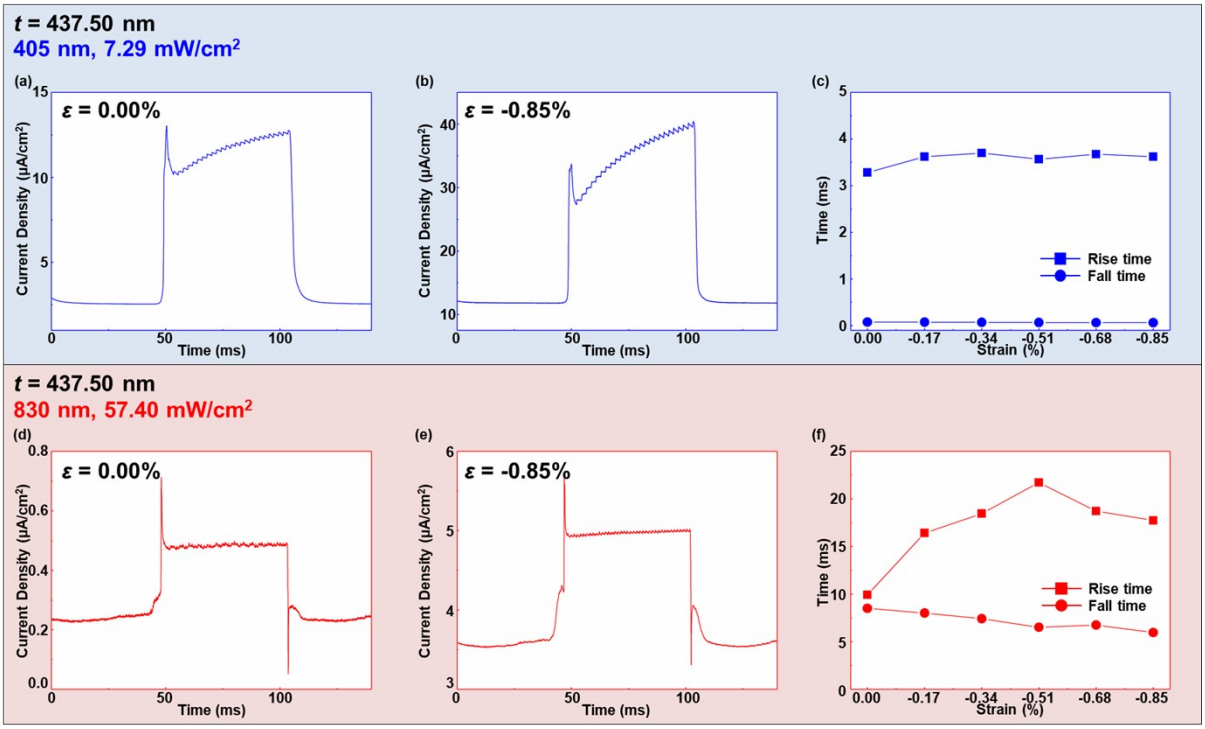

Figure S12. Transient photoresponse characteristics of DUT3. Under 405 nm laser illumination: **a** ε = 0.00%, **b** ε = -0.85%, and **c** rise and fall time as a function of externally applied compressive strain. Under 830 nm laser illumination: **d** ε = 0.00%, **e** ε = -0.85%, and **f** rise and fall time as a function of externally applied compressive strain. (Symbols of different shapes representing rise and fall times, respectively.)

F. Electrical stabilities of p-Si/i- ZnO thin film/n-ZnO nanowires array photodiodes

The current density of DUT1, DUT2, and DUT3 under a reversed bias of -2 V is measured when a stepping motor is repeatedly applying a compressive force of ~3 N to the device at a frequency of 0.5 Hz for 200 s, respectively. Each mechanical forced/force-free trial the device has undergone is defined as a "cycle", and each device has been tested continuously for about 100 cycles. In order to clearly observe the variation in current density when the external compressive force is applied/cancelled to DUT1, DUT2, and DUT3 under

each illumination condition (*i.e.,* dark, 405 and 830 nm laser illuminations, respectively), a continuous 10 cycles of forced/force-free trial that last 20 s are trimmed from the original data and demonstrated in Figure S13, S14 and S15, respectively. In these figures, variations in current density between forced/force-free states are quite distinguishable, showing that the responses of the devices to externally applied compressive force are quite fast. The electrical performance of each device is also very stable and no deterioration in current density (whether it is under forced or force free condition) is observed. After undergoing 100 cycles of trials, no damages or fractures is found in any devices. It is fair to conclude that the device has good stability and reproducibility.

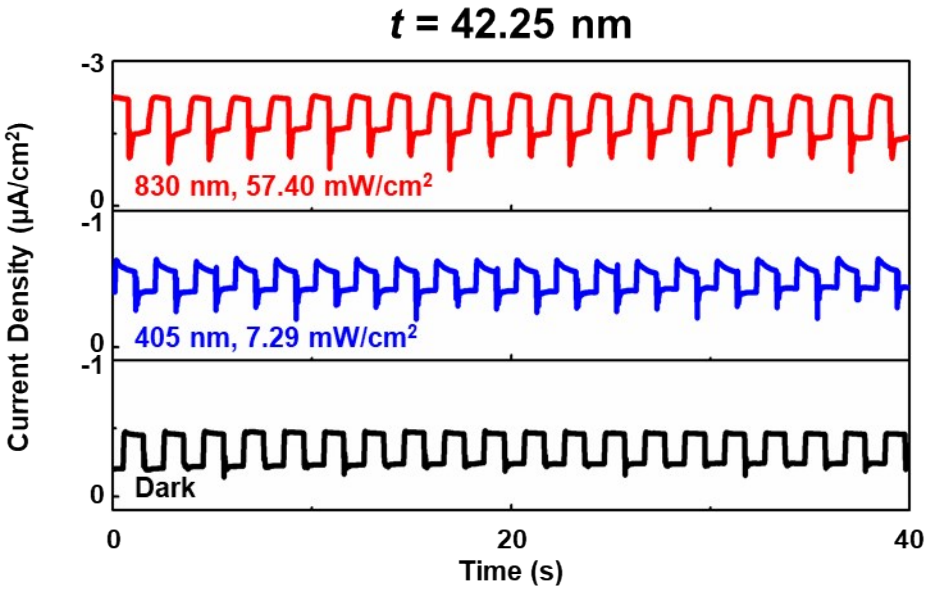

Figure S13. Electrical stability of DUT1 under repeatedly applied compressive force of 3 N. (Lines of different colors representing different illuminating conditions.)

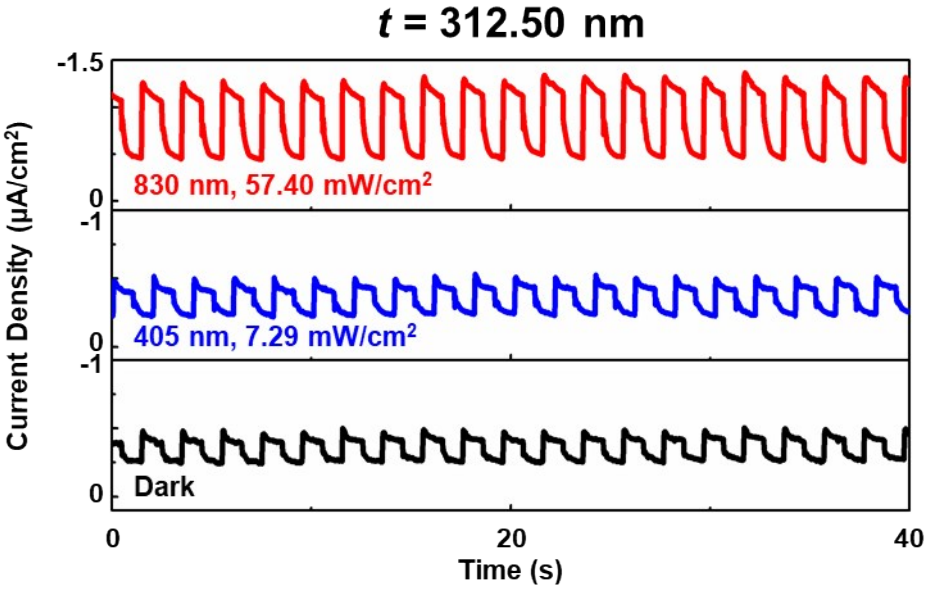

Figure S14. Electrical stability of DUT2 under repeatedly applied compressive force of 3 N. (Lines of different colors representing different illuminating conditions.)

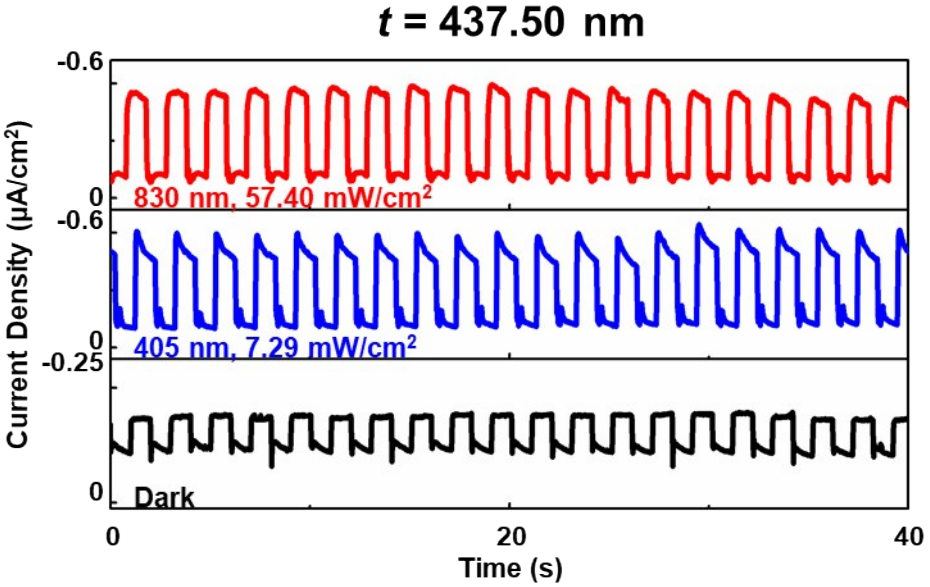

Figure S15. Electrical stability of DUT2 under repeatedly applied compressive force of 3 N. (Lines of different colors representing different illuminating conditions.)

References:

1. S. Xu and Z. L. Wang, *Nano Res*, 2011, **4**, 1013-1098.